Modeling of Ultrawidely Tunable Vertical Cavity Air-Gap Filters and VCSELs

Cornelia Prott, Friedhard Römer, Edwin O. Ataro, Jürgen Daleiden, Sören Irmer, *Student Member, IEEE*, Amer Tarraf, and Hartmut Hillmer

***Abstract*—Tunable vertical cavity devices including an air-gap integrated in the cavity have been designed, fabricated, and investigated. The ultrawide wavelength tuning is realized by micromechanical actuation of Bragg mirror membranes. Based on optical and mechanical model calculations, the air-gap filters and vertical cavity surface emitting lasers (VCSELs) are designed for investigating mainly the optical tuning efficiency. In our research, we focus on two different mirror material systems, dielectric Si_3N_4/SiO_2 and InP/air-gap Bragg mirrors and on two tuning concepts, respectively. For the dielectric mirrors, continuous tuning is achieved by thermal actuation of the Si_3N_4/SiO_2 mirror membranes, and for InP/air-gap mirrors, electrostatic actuation of the InP membranes is used. To verify the optical and mechanical simulations, InP/air-gap filters are characterized by measuring reflectance spectra and the tuning behavior. The measured results agree with the simulations used to optimize the micromechanical and optical characteristics of air-gap filters and VCSELs for optical communication applications.**

***Index Terms*—Air-gap devices, electrostatic actuation, modeling, microoptoelectromechanical system (MOEMS), optical device design, tunable filter, tunable vertical cavity surface emitting laser (VCSEL), vertical cavity devices, WDM.**

I. Introduction

TUNABLE vertical cavity air-gap devices combine the disciplines of optoelectronics and micromechanics to enable novel device features and additional functionalities. To achieve this goal, surface micromachining is used to implement air-gaps and flexible Bragg mirror membranes, which are the key elements of tunable vertical cavity surface emitting lasers (VCSELs) and Fabry–Pérot filters. With micromechanical actuation of the mirror membranes, very efficient ultrawide continuous wavelength tuning is achieved with only a single control parameter [1]. This device feature, attained by microoptoelectromechanical system (MOEMS) technology, is very attractive for advanced optical communication systems based on wavelength division multiplexing systems. Devices with a tuning range covering the 1.5–1.6-μm range of the C and L band allow a considerable reduction of inventory costs, if the high number of currently used nontunable filters and lasers can be replaced. This cost reduction is an advantage in long-haul networks with dense wavelength division multiplexing (DWDM) systems as well as in metropolitan area networks with coarse wavelength division multiplexing systems. Presently, the first widely tunable lasers are projected to incorporate in metro networks as well as in DWDM systems in the near future [2].

In VCSELs and Fabry–Pérot filters, the resonant microcavity is enclosed between two highly reflective mirrors, namely distributed Bragg reflectors (DBR) with a required reflectivity of more than 99.8%. In Fabry-Pérot filters the high quality mirrors with low absorption enable minimized insertion loss and thus a small full width of half maximum (FWHM) of the filter resonance wavelength. For VCSELs, the high reflectivity ensures a high resonator quality, increasing the number of photon circulations, since the amplification per circulation is very small in a vertical cavity laser. In the past, several mirror material systems and technologies have been applied. Most of the current long-wavelength VCSELs on InP substrates are not tunable and feature wafer-fused AlAs/GaAs or AlGaAs/GaAs DBRs [3]–[5], metamorphic AlGaAs/GaAs DBRs [6], [7], monolithic DBRs with GaInAsP/InP [5], [8], AlGaInAs/AlInAs [9], [10], or AlGaAsSb/AlAsSb [11], dielectric mirrors, e.g. Si_3N_4/SiO_2 [8], [12], $MgF_2/\alpha-Si$ [9], or $Al_2O_3/\alpha-Si$ [10], and recently InP/air-gap DBRs [13]–[15]. For all the semiconductor mirrors, whether fused or metamorphic or monolithic, many Bragg periods of 25 up to 50 layers are necessary for the high reflectivity due to the relatively low refractive index contrast achievable in the semiconductor materials. This requires expensive technologies and is difficult to implement. With dielectric DBRs, a higher refractive index contrast is achievable and thus, less layer periods are needed. A second advantage is the low cost and simple fabrication of dielectric materials. However, the highest refractive index contrast is obtained by semiconductor/air-gap DBRs: Using InP membranes only three Bragg periods are sufficient for highly reflective mirrors. Therefore, the reduced semiconductor material and growth process time, as well as applying a batch process and avoiding subsequent micromounting enable as well cost effective and economic mass production. Our concept combines these three features.

For tunable vertical cavity filters or VCSELs, a few implementations of air-gaps in the cavity have been reported. Based on GaAs in the short-wavelength range, electrostatic tuning is demonstrated for Fabry–Pérot filters, as well as VCSELs achieving tuning ranges of 18 and 32 nm, for instance [16]–[18]. For 1.55-μm wavelength, tunable Fabry–Pérot filter concepts based on electrostatic or electrothermal actuation

Manuscript received December 16, 2002; revised June 19, 2003. This work was supported in part by the BMBF funding under Contract 01BC150, in part by the German DFG under Contract Hi 763/3-1, and in part by the European IST TUNIVIC research project.

The authors are with the Institute of Microstructure Technologies and Analytics (IMA) and the Center for Interdisciplinary Nanostructure Science and Technology (CINSaT), University of Kassel, D-34132 Kassel, Germany (e-mail: prott@uni-kassel.de).

Digital Object Identifier 10.1109/JSTQE.2003.818848

[19]–[27] and electrostatically tunable VCSEL with tuning ranges of 31.6 to 50 nm [28], [29] have been reported.

In general, investigations concerning the laser design and structure optimization are based on self-consistent model calculations including carrier transport, optical waveguide properties, heat flux, electrooptical and strained QW gain modeling. For the micromechanically tunable vertical cavity air-gap devices, in addition, the mechanical properties are very important for the device functionality and design. However, since the development of these tunable air-gap devices started just a few years ago, design investigations with model calculations have been rarely reported up to now. Tunable air-gap devices with $Al_2O_3/GaAs$ mirrors have been analyzed recently using a simplified analytical optomechanical model to study the spectral linewidth dependence on mirror deformations [30].

In this paper, we investigate micromechanically tunable air-gap Fabry–Pérot filter and VCSEL devices using combined mechanical and optical model calculations. Our research is focused on two Bragg mirror material systems: InP/air-gap and dielectric mirrors with Si_3N_4 and SiO_2 layers. The tuning concepts are based on electrostatic and thermal actuation of the mirror membranes.

Tunable filters were designed, fabricated, and measured. With InP/air-gap mirrors using the electrostatic tuning principle a record tuning range of 142 nm has been achieved with a low voltage of only 3.2 V. The mechanical and optical model calculations are verified by comparing the results with measured electrostatic tuning results. Based on the optical simulations, the tuning behavior of filter and VCSEL devices for optical pumping as well as the spectral filter linewidth has been investigated.

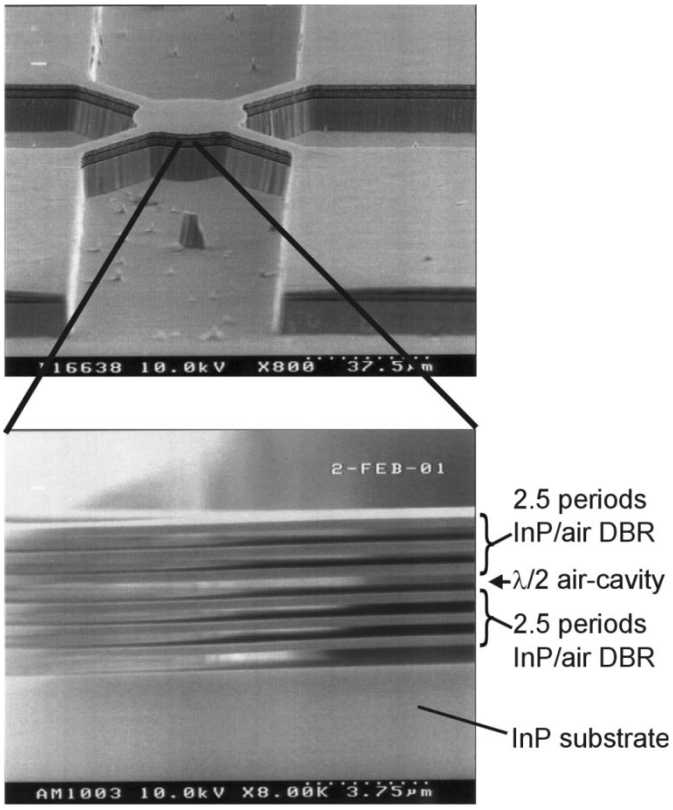

Fig. 1. Scanning electron micrographs of an InP/air-gap filter with three membranes per mirror and four suspensions.

II. Device Structure

A. Air-Gap Filter and VCSEL Design

Our vertical cavity air-gap devices consist of a microcavity embedded between two highly reflective Bragg mirrors. On the one hand, we use dielectric DBRs with Si_3N_4 and SiO_2 layers. One advantage of this material system is the simple and low-cost fabrication by plasma enhanced chemical vapor deposition (PECVD) [31]. On the other hand, InP/air-gap mirrors are used. They are fabricated by surface micromachining techniques. The first process step is growing InP/GaInAs layers by metal organic vapor phase epitaxy. The second step is the definition of the lateral filter structure by dry etching; the GaInAs serve as sacrificial layers. In the third step, they are removed by selective chemical wet etching with $FeCl_3 + H_2O$ to obtain the air-gaps [23], [32].

The lateral filter or VCSEL structure features circular-shaped mirror membranes with several suspensions and supporting posts. An example of a multiple air-gap/InP filter with three InP membranes per mirror is shown in Fig. 1, where the diameter of the membranes is 40 μm, the suspension length in the displayed sample is 30 μm, whereby this length varies between 10 and 80 μm in our devices. The InP thickness of the membranes is $d_{InP} = 357$ nm, the mirror air-gaps are $d_{air} = 375$-nm-thick, and the air-cavity is $L_{air} = 830$ nm.

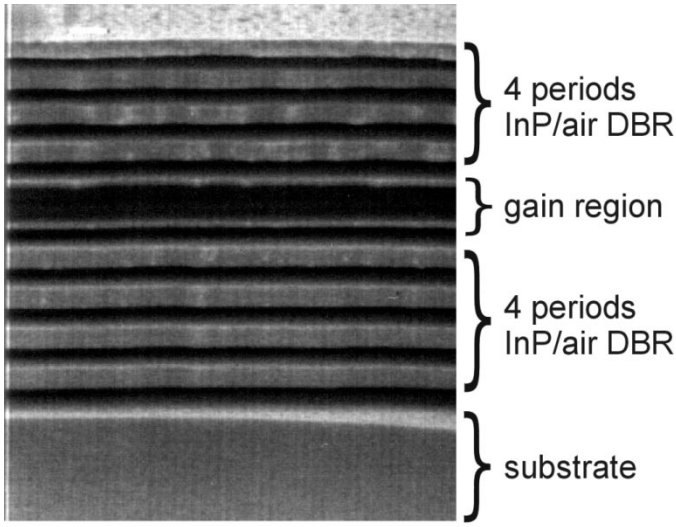

Fig. 2. Scanning electron micrograph with a detailed view of an InP/air-gap VCSEL structure with four membranes per mirror.

The VCSEL structures are based on the filter design with an additional active region embedded in the microcavity. They are designed at first for optical pumping. In Fig. 2, a detailed view of an air-gap VCSEL layer structure is presented. The Bragg mirrors consist of four InP membranes and the active region has three pairs of QW layers.

The resonator quality depends on the refractive index contrast between the Bragg mirror layer materials, on the absorption and

on the number of periods. For the dielectric mirrors, the optical material parameters depend significantly on the PECVD process parameters. Using spectroscopic ellipsometry, we measured, for our standard process, the wavelength dependence of refractive index and absorption coefficient to be considered in our device modeling. The measured values of the refractive index at 1.55 μm are $n_{\mathrm{Si3N4}} = 1.932$ and $n_{\mathrm{SiO2}} = 1.469$, and the values of the absorption coefficient are $\alpha_{\mathrm{Si3N4}} \leq 3\ \mathrm{cm}^{-1}$ and $\alpha_{\mathrm{SiO2}} \leq 1\ \mathrm{cm}^{-1}$ for Si_3N_4 and SiO_2, respectively. With this high refractive index contrast, 12-layer periods are required per DBR, ensuring a high reflectivity of more than 99.8%. The advantage of InP/air-gap Bragg mirrors with $n_{\mathrm{InP}} = 3.167$ and $n_{\mathrm{air}} = 1$ is an even much higher refractive index contrast of $\Delta n = 2.167$. Thus, only three layer periods are necessary for the same value of reflectivity.

B. Tuning Principles

For both material systems, the ultrawide continuous tuning is achieved by micromechanical actuation of the mirror membranes, but with two different tuning principles. For the Si_3N_4/SiO_2 mirrors, electrothermal actuation is used and, for the InP/air, electrostatic actuation is used. Both tuning principles are demonstrated in Fig. 3. The dielectric mirrors have meanderlike chromium thin-film heaters deposited on the suspensions. Actuation of the top mirror membrane can be obtained by thermal expansion of the heated suspensions [Fig. 3(a) left]. This actuation results in a change of the cavity length and, therefore, the filter resonance wavelength is tuned.

In the case of semiconductor/air-gap structures, the membranes of one Bragg mirror are n-doped and the other mirror membranes are p-doped forming a pin-diode including the intrinsic cavity GaInAs sacrificial layer residual in the supporting posts. When applying a reverse bias very efficient tuning is achieved by electrostatic actuation of the two InP membranes embedding the cavity [Fig. 3(a) right]. Thus, the filter transmission peak (or resonance wavelength) shifts to shorter wavelength with increasing reverse bias as demonstrated in Fig. 3(b). Thereby, the reason for the high efficiency of this tuning method is the device miniaturization and the remaining significant part of electrostatic force during the scaling down to nanoworld dimensions [1].

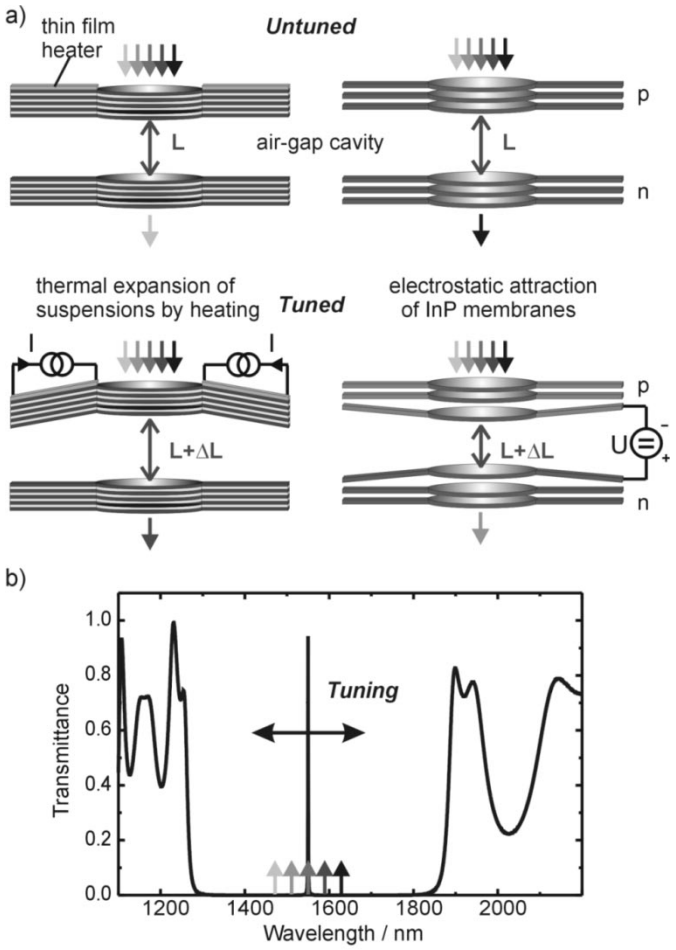

Fig. 3. Micromechanical tuning principles: (a) thermal actuation (left) and electrostatic actuation (right) of mirror membranes and (b) resulting tuning of the resonance wavelength (filter peak) within the transmittance spectrum.

III. Experimental Results of InP/Air-Gap Filters

For the experimental characterization, reflectance spectra of various InP/air-gap filters were measured using a single mode (SM) fiber setup [26]. An erbium-doped fiber amplifier was deployed as a white light source and the reflected light was coupled directly into the SM fiber and measured with an optical spectrum analyzer. We studied InP/air-gap filter structures with the geometry described previously. An air-gap cavity is embedded between two 2.5 periods InP/air Bragg mirrors appropriating three InP membranes with a diameter of 20 or 40 μm. In this paper, measured reflectance spectra are presented with 40 μm membranes held by three or four suspensions with a length of 20 to 40 μm.

Fig. 4 presents measured reflectance spectra of two different InP/air filters with applied tuning voltages. The top figure shows the tuned reflection dip for a filter with three 30-μm suspensions showing a tuning range of $\Delta\lambda = 127$ nm with a voltage of only 7.3 V [1], [26]. The FWHM of the filter dip decreases during tuning from 7.5 to 3.5 nm.

The bottom graph in Fig. 4 demonstrates measured spectra of a structure featuring four suspensions with 40-μm length. With a very low voltage of 3.2 V, a record tuning range of $\Delta\lambda = 142$ nm is achieved [32], [33]. The FWHM of the filter dip increases with tuning from 3.5 to 4.5 nm. Reasons for the increase or decrease of the dip linewidth during tuning are discussed in the next chapter of optical model calculations.

IV. Device Modeling of Air-Gap Filter Tuning

The efficiency of the ultrawide continuous tuning in vertical cavity devices depends on both the mechanical properties of the InP membranes and the optical properties of the multilayer structure. For investigations and design of the micromechanical tuning behavior, we performed basic optical and mechanical model calculations. The results on air-gap filters are presented in the following two sections. In the third section, the combined optical and mechanical simulations are compared with the measured tuning behavior. The device modeling of VCSELs based on these verified tools is presented in the next chapter.

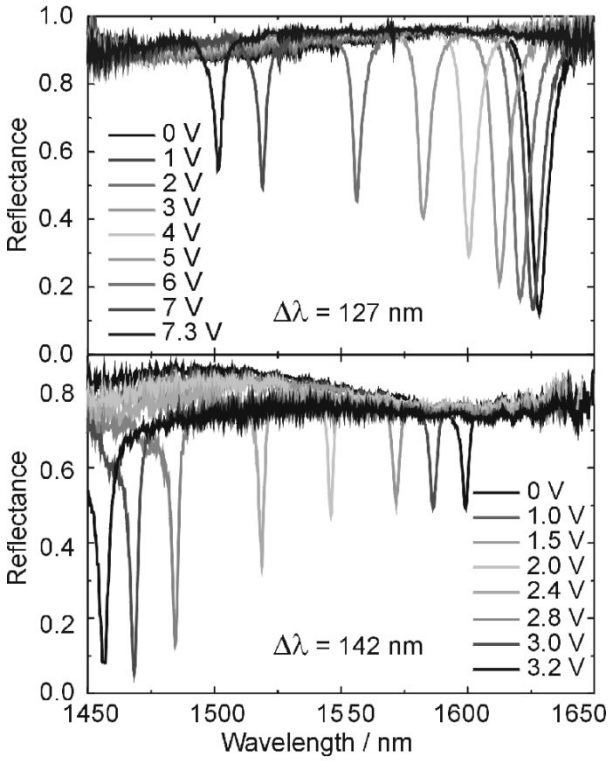

Fig. 4. Measured reflectance spectra of two different InP/air-gap filter structures. Top: filter with three suspensions of 30-μm length and applied tuning voltages up to 7.3 V resulting in a tuning range of $\Delta\lambda = 127$ nm. Bottom: filter with four suspensions of 40-μm length and applied tuning voltages up to 3.2 V resulting in a record tuning range of $\Delta\lambda = 142$ nm.

A. Optical Model Calculations

The basic model for describing the transmission and reflection of light at interfaces is the scattering theory using matrix formalism for the linear relation of light input and output. This enables a very convenient description of lightwave propagation through multiple layer structures by using matrix multiplication. Thereby, all layers and interfaces are described with matrices using the layer thickness and the optical parameters as the refractive index and absorption. In multilayer structures, e.g., in DBRs, forward and backward traveling lightwaves interfere constructively or destructively. In vertical cavity devices, a standing photon wave is generated at the wavelength of constructive interference $\lambda_{\rm res}$ (resonance wavelength). For optical model calculations of our filters and VCSELs, we used this transfer matrix method [34] based on the one-dimensional (1-D) scattering theory in axial direction. To investigate and optimize the optical tuning efficiency, the 1-D transfer matrix method is a very suitable and effective tool, whereas solving the full three-dimensional (3-D) waveguide equation is a very complicated method. However, such two-dimensional (2-D) or 3-D simulations are necessary for investigations of all feasible optical eigenmodes in the vertical resonator and their modal irradiations and losses, especially in the case of bent mirror membranes [36].

Using the 1-D transfer matrix method, we first calculated for our air-cavity filters the electric field distribution corresponding to the photon wave at the resonance wavelength $\lambda_{\rm res}$ and, second, the reflectance spectrum. Based on these simulations we compared filters with a 1/2 $\lambda_{\rm res}$ air-cavity

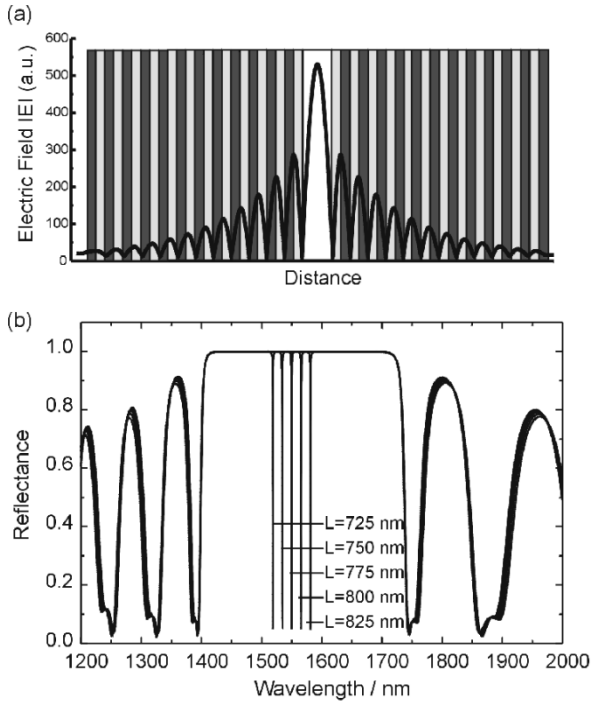

Fig. 5. Transfer matrix simulations of a Si_3N_4/SiO_2 air-cavity filter: a) layer structure and electric field distribution of the photon wave and b) reflectance spectra resulting in an optical tuning efficiency of $\Delta\lambda/\Delta L = 0.63$.

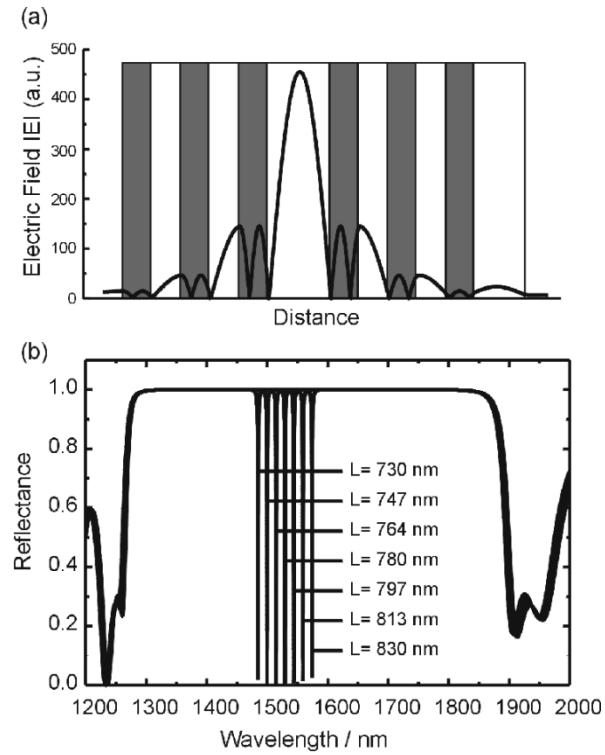

Fig. 6. Transfer matrix simulations of an InP/air-gap filter. (a) Layer structure and electric field distribution of the photon wave. (b) Reflectance spectra resulting in an optical tuning efficiency of $\Delta\lambda/\Delta L = 0.8$.

embedded between two mirrors of: 1) 12 periods Si_3N_4/SiO_2 and 2) 3-periods InP/air-gap. The results are presented in Figs. 5 and 6, respectively.

Fig. 5(a) displays the dielectric air-cavity filter structure with 1/4 λ_{DBR} layers of Si_3N_4 and SiO_2 for a Bragg mirror center wavelength of $\lambda_{\mathrm{DBR}} = 1.55\ \mu$m and the corresponding electric field distribution. In the calculated reflectance spectra figured in Fig. 5(b), the tuning is considered by varying the air-cavity length L between 725 and 825 nm. All spectra show a Bragg mirror stopband of 300-nm width nearly unaffected by the varied cavity length. However, the filter resonance wavelength tuning is $\Delta\lambda = 62.6$ nm with $\Delta L = 100$ nm. Therefore, an optical tuning efficiency of $\Delta\lambda/\Delta L = 0.626$ is obtained for this dielectric air-cavity filter.

Fig. 6 shows the corresponding results for a multiple air-gap/InP filter with 3/4 λ_{DBR} InP membranes and 1/4 λ_{DBR} mirror air-gaps, for a center wavelength of $\lambda_{\mathrm{DBR}} = 1.50\ \mu$m. In Fig. 6(b), the stop band of the Bragg mirrors covers a very wide range of 600 nm. Therefore, we chose the lower center wavelength to shift this wide stop band to cover also the 1.3-μm wavelength range. This is an optimized feature especially for optical fiber communication in the 1.55-μm range with simultaneous total reflection of the 1.3-μm wavelength. For tuning investigations, the reflectance spectra are calculated for the same air-cavity length variation $\Delta L = 100$ nm, whereas L is changed between 830 and 730 nm. Considering that only the inner membranes are deflected by electrostatic tuning, this results in a tuning range of $\Delta\lambda = 80$ nm. Otherwise, if all membranes would be actuated, the tuning range would be $\Delta\lambda = 89$ nm. Compared to the dielectric filter, a better optical tuning efficiency of $\Delta\lambda/\Delta L = 0.8$ is achieved with this InP/air-gap filter.

In the measured reflectance spectra, broad filter dips with a FWHM of 3.5 to 7.5 nm were observed, whereas the 1-D optical simulations predict a FWHM of 1 nm for these filters. One reason for the higher measured spectral linewidth is a small bending of the mirror membranes due to residual stress in the epitaxial InP layers [35]. This causes a widening of the incident Gaussian beam during the multiple reflections within the cavity and leads to lateral irradiations and cavity losses entailing a broadening of the filter dip. In the 1-D optical simulations, these irradiations are not considered. However, with a multidimensional simulation tool, several 3-D eigenmodes as well as their irradiations are determined for ideal planar and bent filter membranes [36]. Considering these cavity losses the FWHM values for the several vertical eigenmodes are higher than 1 nm, depending on the lateral irradiation losses for each mode. For the first mode with the smallest irradiation losses, e.g., an FWHM of 1.5 nm is obtained for planar membrane filters with 3-D simulations.

A second and more important reason for the observed difference of the calculated and measured linewidth is that the spectral mode spacing is in the 1-nm range and two or three modes are overlapping, forming the broadened filter dip in the measured spectra. In the measurement setup, the incident Gaussian beam is able to excite several modes within the filter cavity, the fundamental mode normally with the highest efficiency and the higher order modes less.

In the measurements, a considerable decrease or increase of the filter dip linewidth during tuning was observed. One reason for this is a tuning induced small deformation of the mirror membranes in such a way that the parts of the higher order modes diminish. This is observed for the three suspension filter and for high voltages a small shoulder of higher order modes remains on the left filter dip side. In the other case of the four suspensions filter, the tuning generates a small deformation of membranes in such a way that the number of excitable modes increases.

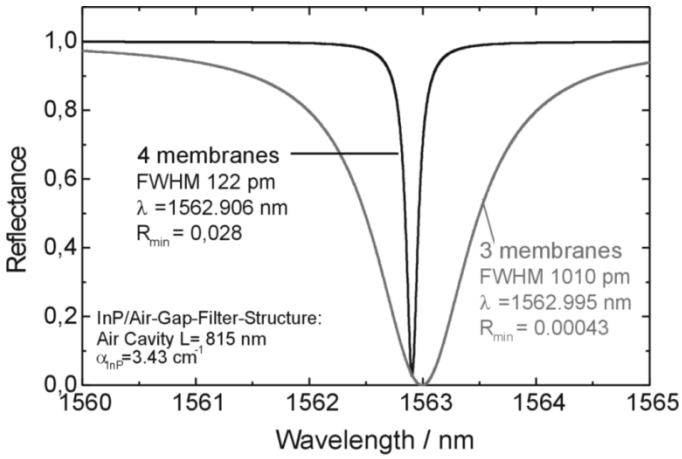

Fig. 7. FWHM of an InP/air-gap filter with three and four membranes per mirror.

For optical communication applications, a small spectral linewidth of devices is required, particularly for DWDM systems. A significant reduction of the spectral filter linewidth can be achieved by increasing the reflectivity of the mirrors, hence, by using more layer periods in the mirrors. This is demonstrated in Fig. 7, which shows reflectance spectra in a zoomed wavelength range around the filter dip calculated with the 1-D transfer matrix method. The filter dips are compared for the implemented and measured InP/air-gap filter with 3 InP membranes per mirror and for a structure with four membranes. With the additional membrane per mirror, the FWHM of 1 nm is reduced to 122 pm. Due to the marginal absorption in the InP layers ($\alpha_{\mathrm{InP}} = 3.43\mathrm{cm}^{-1}$), a small shift of the dip wavelength is observed and a small increase of the minimum reflectance of the dip.

B. Mechanical Model Calculations for Electrostatic Tuning

For complete investigation of the tuning efficiency, we determined the achievable deflection of the mirror membranes. In this paper, we concentrate on the electrostatic tuning method of InP/air-gap devices. Based on a 3-D structural mechanics model, we studied the electrostatic actuation with the finite element method (FEM) [37], [38]. By the structural mechanics model, material deformations generated by stress or external forces acting on the material are described. Based on the static equilibrium conditions between the stress matrix σ and the volume force density f and Hooke's law for elastic materials the following equations system has to be solved [38]:

$$-\sum_j \left[\frac{\partial}{\partial x_j} G\left(\frac{\partial u_i}{\partial x_j} + \frac{\partial u_j}{\partial x_i}\right) + \frac{\partial}{\partial x_i}\left(\mu \frac{\partial u_j}{\partial x_j}\right)\right] = f_i \quad (1)$$

where x_i and $x_j (i, j = 1, 2, 3)$ denote the space coordinates of the vector $x = (x_1, x_2, x_3)$, u_i, and u_j the deformation compo-

nents of deformation vector $\boldsymbol{u}(x) = (u_1, u_2, u_3)$, G is the shear modulus

$$G = \frac{E}{2(1+\nu)} \tag{2}$$

and μ the Lamé constant results from

$$\mu = \frac{E\nu}{(1+\nu)(1-2\nu)} \tag{3}$$

including Young's modulus E and the Poisson ratio ν, with values of $E = 61.06$ GPa and $\nu = 0.357$ for InP [39].

In our tunable InP/air-gap devices, an applied voltage U generates the electrostatic force F_{el} acting on the InP membrane surface. This is considered by the force [40] per area A

$$f_{\mathrm{el}} = \frac{F_{\mathrm{el}}}{A} = \frac{\varepsilon_0 U^2}{2\big(L_0 - \Delta L(x)\big)^2} \tag{4}$$

where L_0 is the nontuned cavity length and $\Delta L(x)$ denotes the resulting change of the cavity length due to the elastic deflection of the membrane. In our filter structures, the two interior InP membranes are actuated symmetrically and the change of the cavity length is two times the deflection of one membrane $\Delta l(x)$, considered with $\Delta L(x) = 2\,\Delta l(x)$.

To investigate the tuning behavior, the deflection is calculated recursively with 3-D FEM analysis and the results are depicted qualitatively for one filter structure example in Fig. 8(a). The simulations show a strong bending of the suspensions, whereas the membranes remain nearly planar in the center with only a small curvature of the membrane margin. The mechanical properties of the InP membranes and suspensions, namely the flexibility and the spring properties, are determined by the geometry of the filter structure and by the material parameters. Hence, for detailed tuning investigations, the geometric parameters are varied. The first parameter to be varied is the suspension length for a filter structure with four suspensions of 10-μm width, a membrane diameter of 40 μm, and a layer thickness of 357 nm for the membrane and suspensions. The membrane center deflection Δl_c is determined and the resulting changes of the cavity length is $\Delta L = 2\,\Delta l_c$. Combined with the tuning efficiency $\Delta\lambda/\Delta L = 0.8$ obtained by the optical calculations described above, the wavelength tuning $\Delta\lambda$ is defined and plotted versus the applied voltage in Fig. 8(b). The results of our theoretical model calculations are compared for suspension lengths of 20, 30, and 40 μm, showing the most efficient tuning for the long suspensions. Filters with suspensions of length $l_{\mathrm{susp}} = 20$ μm result in $\Delta\lambda = 61$ nm for an applied voltage of 8 V, whereas using $l_{\mathrm{susp}} = 30$ μm, the same tuning range is achieved for 4.7 V, and with $l_{\mathrm{susp}} = 40$ μm, only 2.8 V is necessary. Among the three samples, the best electrostatic tuning efficiency is obtained with the 40 μm suspensions, e.g., $\Delta\lambda = 140$ nm is obtained at 3.7 V tuning voltage.

Generally, it is possible to achieve these tuning values also for the 20 and 30-μm suspensions, but for higher voltages. However, the tuning range is limited by the "pull-in" instability of the actuated membranes. The reason for this is the nonlinear electrostatic force is as in (3), which depends on the cavity length with $1/L^2$, whereas the elastic restoring force of the membrane

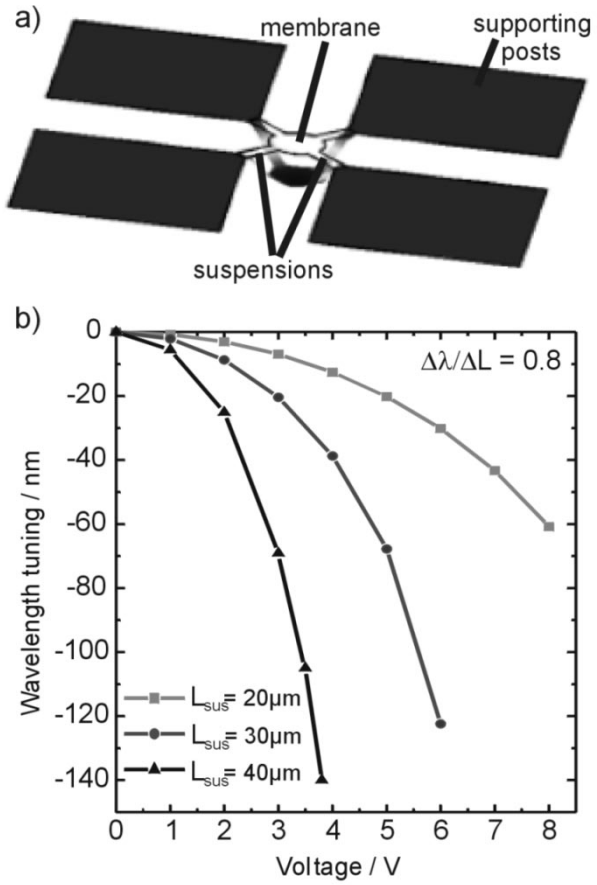

Fig. 8. (a) Qualitative FEM simulation of an InP membrane and the electrostatic actuation (b) resulting wavelength tuning of combined optical and mechanical simulations for filters with varied suspension lengths.

is linear with L using an analytical mechanical model [40], [41]. Therefore, increasing the tuning voltage across the membranes results in a fast-growing electrostatic force, which exceeds the elastic restoring force. The force equilibrium determines the maximum possible membrane actuation prior to the pull-in instability occurs related to the pull-in voltage. Analytical mechanical model calculations lead to a maximum change of the cavity length $\Delta L_{\max} = 1/3\ L_0$ [26], [41]. Therefore, $\Delta L_{\max}$ depends only on the initial cavity length L_0 but not on other geometric parameters.

Additional simulations on filter structures with two and three suspensions result in a considerably increased actuation efficiency with a decreased number of suspensions. Therefore, two long suspension would be preferable for an optimized electrostatic actuation of the filter membranes, but the technological implementation of stable filter structures without strain-induced deformations is very difficult for less or long suspensions. Furthermore, filter structures with long suspensions are more sensitive to thermal and mechanical instabilities. InP/air filters with 2, 3, and 4 suspensions having a length of 10 to 80 μm have been implemented. Optical measurements show a filter tuning up to 40 μm long suspensions, however.

C. Comparison of Simulations and Measurements

The results of the combined mechanical FEM and optical simulations are compared to measured tuning behavior of sev-

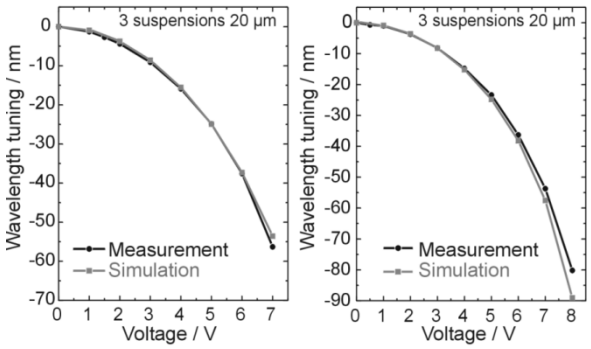

Fig. 9. Comparison of measured and calculated tuning versus applied voltage for two InP/air-gap filters with 3 suspensions of 20-μm length.

eral filter devices. In Fig. 9, a comparison of measured and calculated wavelength tuning $\Delta\lambda$ versus applied voltage is figured for two different filters. Both examples have three suspensions of 20-μm length, but slightly different cavity thicknesses of $\mathrm{L}_1 = 840$ nm (left) and $\mathrm{L}_2 = 860$ nm (right), showing nearly identical tuning behavior. The simulations show an excellent agreement with the measurements. To determine $\Delta\lambda$, the optical tuning efficiency is calculated using the previously described 1-D optical model. A very good agreement between simulations and measurements is also obtained for other filter structures with different geometries and suspension lengths. These investigations demonstrate that the combined mechanical FEM and the optical simulations fulfill the requirements to calculate the tuning behavior as a function of applied voltage for device structures with an arbitrary geometry. For this tuning prediction, only material parameters and the device geometry is required without involving any fit parameter from measurements. Such a curve fitting would be necessary for analytical mechanical model calculations, e.g., based on a linear spring model using a spring constant as fit parameter. In conclusion, we demonstrated that the model calculations are a suitable tool for a design optimization of vertical cavity devices. In the next chapter, we use this tool for an optimization of the tuning behavior of air-gap VCSELs.

V. Device Modeling of Tunable Air-Gap VCSELs

The results obtained for the air-gap filters are extended to the VCSEL-design optimization. The mechanical properties of the InP membranes during tuning is transferable exactly to electrostatically tuned VCSELs, but the optical tuning properties depend on the multiple layer structure and the cavity length. Thus, they are different from filter tuning behavior and they vary extremely with the VCSEL design. In the following sections, the optical tuning efficiency of VCSEL structures is investigated and again the two material systems are compared.

A. Air-Gap VCSELs With Dielectric Mirrors

First, VCSELs with two dielectric Bragg mirrors defining the cavity are discussed. The cavity includes a 1/2 λ_{res} air-gap ($\lambda_{\mathrm{res}} = 1.55$ μm) and a GaInAsP/InP-based active region consisting of a variable number of quantum well active layers. The simulation results of the transfer matrix model are presented in Figs. 10 and 11 for two different VCSEL samples, respectively.

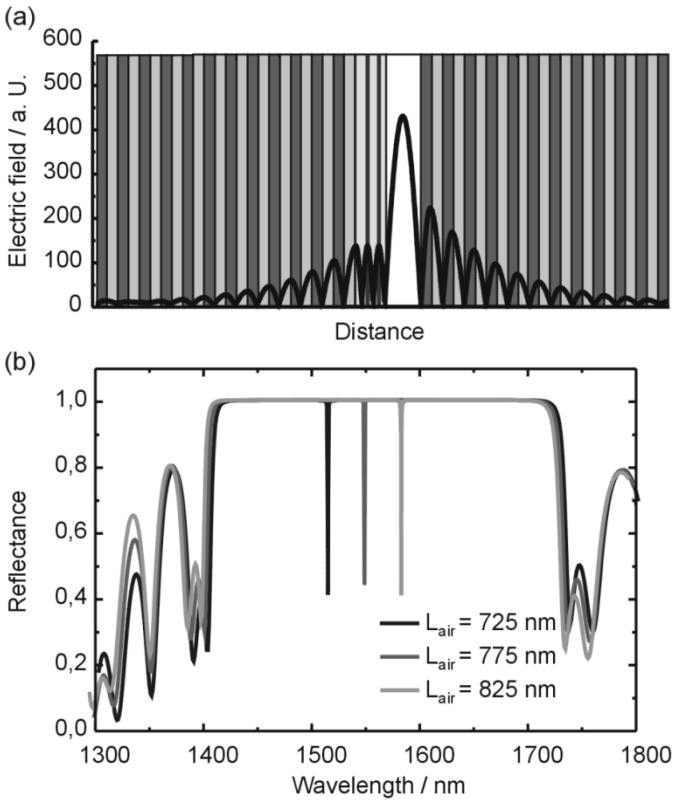

Fig. 10. Simulation results for a VCSEL with $\mathrm{Si_3N_4/SiO_2}$ mirrors and 1.25 λ active region: (a) layer structure and electric field distribution and (b) reflectance spectra resulting in an optical tuning efficiency of $\Delta\lambda/\Delta\mathrm{L} = 0.6$.

One difference is the total thickness of this active region with 1.25 λ_{res} in Fig. 10 and 1 λ_{res} in Fig. 11, respectively. The latter one has an additional 1/4 λ_{res}-thick $\mathrm{Si_3N_4}$ antireflection layer between the air-gap and the active region. In both designs, the left Bragg mirror consists of 12 periods $\mathrm{Si_3N_4/SiO_2}$ and the right one of 11.5 periods $\mathrm{Si_3N_4/SiO_2}$.

In Figs. 10(a) and 11(a), the layer structure as well as the electric field distribution for the resonance wavelength is displayed and in Figs. 10(b) and 11(b), the corresponding reflectance spectra for an air-gap tuning of $\Delta L_{\mathrm{air}} = 100$ nm. For comparing the field strength amplitudes, the results in the model calculations are related to a fixed total power. In optimized VCSEL structures, the position of active layers is in the antinodes of the electric field. The structure with the 1.25 λ_{res}-thick active region includes two QW active layers. The achieved tuning range is $\Delta\lambda = 60$ nm for $\Delta L\mathrm{air} = 100$ m, resulting in a tuning efficiency of $\Delta\lambda/\Delta L_{\mathrm{air}} = 0.6$. In contrast, the structure with the 1 λ_{res} active region (Fig. 11) includes one QW active layer and reveals a smaller tuning range of $\Delta\lambda = 40$ nm and a corresponding tuning efficiency of $\Delta\lambda/\Delta L_{\mathrm{air}} = 0.4$. Compared to the first VCSEL structure, this device has the advantage that, due to the additional $\mathrm{Si_3N_4}$ antireflection layer, the maximum electric field in the QW active layer is twice as high. This ensures a better lasing efficiency per active layer and this compensates the reduced number of QW layers in the VCSEL structure of Fig. 11 compared to that in Fig. 10. However, due to the $\mathrm{Si_3N_4}$ layer, a reduced tuning efficiency is obtained. By increasing the layer thickness of the

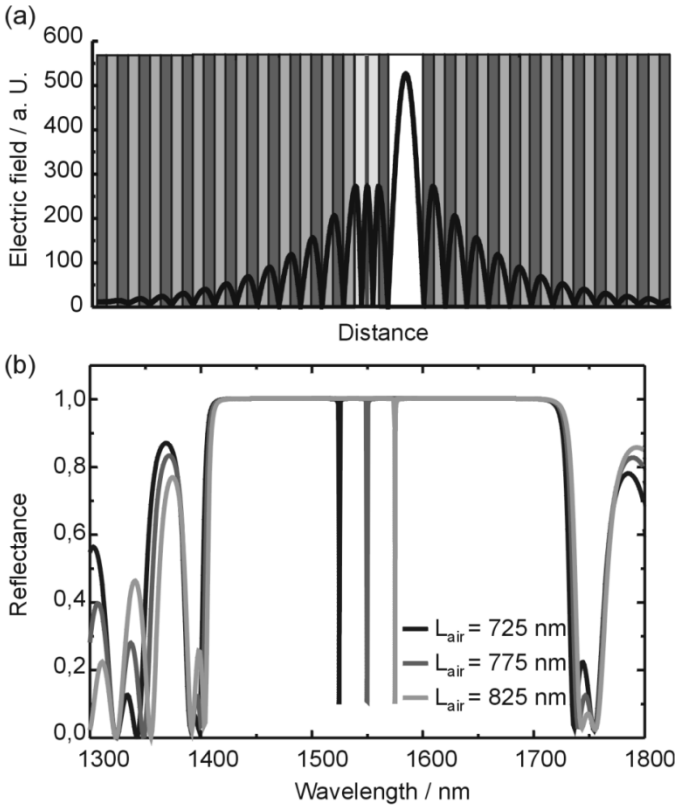

Fig. 11. Simulation results for a VCSEL with Si_3N_4/SiO_2 mirrors and 1 λ active region: (a) layer structure and electric field distribution and (b) reflectance spectra resulting in an optical tuning efficiency of $\Delta\lambda/\Delta L = 0.4$.

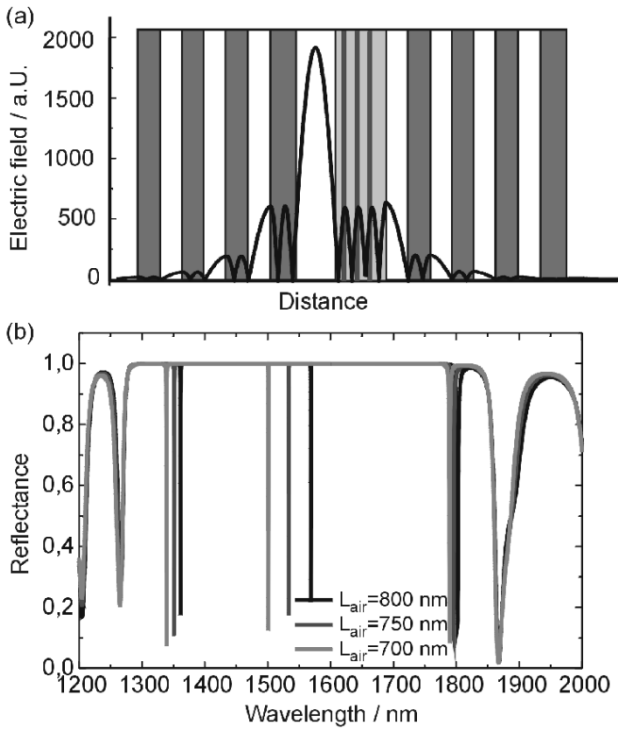

Fig. 12. Simulation results for an InP/air-gap VCSEL with a 1.75 λ active region: (a) layer structure and electric field distribution and (b) reflectance spectra resulting in an optical tuning efficiency of $\Delta\lambda/\Delta L = 0.678$.

active region in 1/2 $\lambda_{\rm res}$ steps, the electric field distribution shows more antinodes, and the number of active layers can be increased simultaneously. However, this results in a reduction of tuning range and efficiency. For three antinodes and QW layers, i.e., an active region thickness of 1.75 $\lambda_{\rm res}$ is necessary without antireflection layer, and a reduced tuning efficiency of $\Delta\lambda/\Delta L_{\rm air} = 0.54$ is obtained. With the antireflection layer, a 2 $\lambda_{\rm res}$ active region implies three antinodes addicted to $\Delta\lambda/\Delta L_{\rm air} = 0.3$. Therefore, a tradeoff between optimization of the tuning efficiency and lasing efficiency is observed.

B. Design of All-Air-Gap VCSELs

In this section, all-air-gap VCSELs with two InP/air mirrors are the main focus. Concerning the tuning efficiency, an optimized structure with four InP membranes per mirror and a 1.75-$\lambda_{\rm res}$ active region is presented in Fig. 12. The electric field distribution in Fig. 12(a) features three antinodes in the active region for three QW layers. The field maxima are considerably higher, compared with the dielectric mirror VCSELs, resulting in a better lasing efficiency per QW layer. In addition, the maximum electric field in the tuning air-gap is higher as well. This enables an enhanced tuning range of $\Delta\lambda = 67.8$ nm for an air-gap thickness variation of $\Delta L_{\rm air} = 100$ nm, as shown in Fig. 12(b). Therefore, the optical tuning efficiency for the all-air-gap VCSEL is better in comparison to the dielectric VCSELs. However, compared with the InP/air-gap filter structures with $\Delta\lambda/\Delta L_{\rm air} = 0.8$ (chapter III.A), the tuning efficiency is decreased due to the enhanced thickness of the cavity including the 1.75 $\lambda_{\rm res}$ active region and the 1/2 $\lambda_{\rm res}$ tuning air-gap. The extremely wide stop bandwidth of 600 nm enables two additional resonance wavelengths to appear around 1350 and 1800 nm, but they are barely tuned.

One disadvantage of an all-air-gap VCSEL is the fact that the active region is enclosed by two air-gaps and, thus, thermally isolated by air. The generated heat during optical pumping and lasing has to be transferred through the suspensions of the active region and therefore, the heat dissipation is rather low, whereas for the dielectric mirror VCSELs the solid mirror structure attached to the active region enables a better thermal behavior and lower temperatures. Based on heat flux simulations the temperature distribution of both VCSEL types is determined for the same heat source conditions. Thereby, a heat source power of 1 mW within an active region of 10-μm diameter generates a temperature increase of $\Delta T = 49.8$ K for the InP/air-gap mirrors and only $\Delta T = 8.1$ K for the Si_3N_4/SiO_2 mirrors. To combine the advantages of both material systems, a mixed air-gap VCSEL is proposed using one dielectric mirror for the heat dissipation and one InP/air-gap mirror for advanced optical tuning efficiency based on electrostatic tuning principle.

C. Design of Mixed Air-Gap VCSELs

The layer structure and the simulation results for this mixed VCSEL are displayed in Fig. 13. In comparison to the all-air-gap VCSEL, the maximum electric field in the active layers, as well as in the tuning air-gap, is lower (with a factor of 2). On the one hand, this fact decreases the expected lasing efficiency and, on the other hand, the optical tuning efficiency. As can be observed in Fig. 13(b) with the mixed VCSEL, a moderate tuning of $\Delta\lambda/\Delta L_{\rm air} = 0.46$ nm is achievable. This is a better tuning

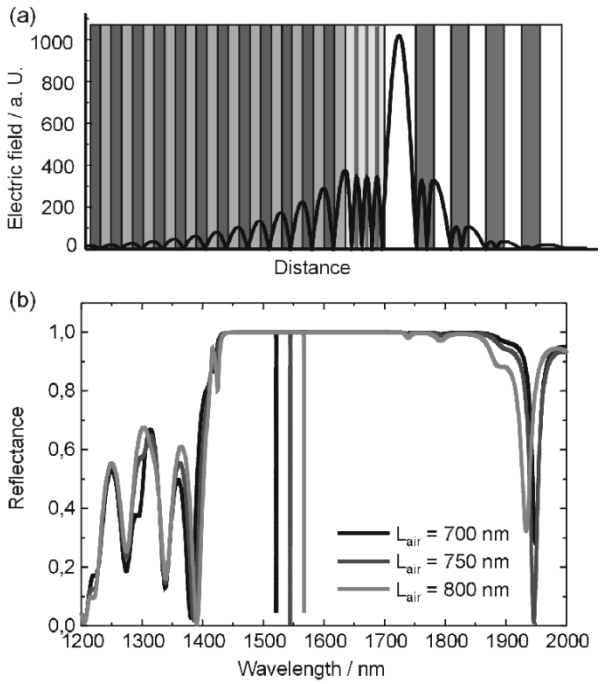

Fig. 13. Simulation results for a VCSEL structure with one InP/air mirror, one Si_3N_4/SiO_2 mirror and a 1.75 λ active region: (a) layer structure and electric field distribution and (b) reflectance spectra resulting in an optical tuning efficiency of $\Delta\lambda/\Delta L = 0.46$.

behavior than a comparable VCSEL with two Si_3N_4/SiO_2 mirrors, an antireflection layer having three QW active layers and a tuning efficiency of $\Delta\lambda/\Delta L_{\text{air}} = 0.3$ nm. Thus, for optimization of the tuning and the thermal properties the mixed VCSEL is a compromised VCSEL structure.

VI. Conclusion

In conclusion we reported on the design optimization of ultrawide tunable vertical cavity air-gap filters and VCSELs mainly for optical communication applications. For the Bragg mirrors two material systems, Si_3N_4/SiO_2 and InP/air, have been compared for filter devices and for VCSEL structures. Two different tuning principles have been presented: thermal tuning for the dielectric and electrostatic actuation of the InP/air-gap filters. Based on combined optical and mechanical model calculations the micromechanical tuning behavior has been investigated. For a vertical cavity filter with 12 periods Si_3N_4/SiO_2 mirrors an optical tuning efficiency of $\Delta\lambda/\Delta L = 0.63$ is obtainable and $\Delta\lambda/\Delta L = 0.8$ nm for an InP/air-gap filter with three InP membranes. Measured reflectance spectra of InP/air filter including electrostatic tuning have been shown ultrawide tuning ranges for several filter samples with different geometries. A record value of $\Delta\lambda = 142$ nm with an applied voltage of only 3.2 V is achieved for a filter with four 40-μm suspensions. The results of the combined optical and mechanical simulation tool show a very good agreement with experimental results. The simulations enable a prediction of tuning behavior by using only material and geometric parameters without any fit parameter. Optical 1-D model calculations for investigating the filter dip linewidth indicated for a filter with three InP membranes per mirror an achievable FWHM of 1 nm. A considerable reduction of linewidth up to $\text{FWHM} = 122$ pm is obtainable by using four InP membranes. The design optimization of air-gap VCSELs with two dielectric mirrors results in optical tuning efficiencies of $\Delta\lambda/\Delta L = 0.3$ to 0.6, depending on the layer structure. The best optical tuning of $\Delta\lambda/\Delta L = 0.678$ is achieved by an all-air-gap VCSEL, but with the disadvantage of a worse thermal behavior and, thus, higher operation temperatures. To meet all of the thermal and optical requirements, a mixed VCSEL with one InP/air and one Si_3N_4/SiO_2 mirror is proposed to profit from the advantages of both material systems. This mixed VCSEL enables a moderate optical tuning efficiency of $\Delta\lambda/\Delta L = 0.46$.

Acknowledgment

The authors thank A. Witzig, S. Schüler, V. Rangelow, M. Strassner, and W. Scholz for simulation and technological support.

References

[1] H. Hillmer, J. Daleiden, C. Prott, F. Römer, S. Irmer, V. Rangelov, A. Tarraf, S. Schüler, and M. Strassner, "Potential for micromachined actuation of ultra-wide continuously tunable optoelectronic devices," *Appl. Phys.*, vol. B 75, pp. 3–13, 2002.

[2] "Agility and Iolon receive tunable laser contracts," *Compound Semiconduct.*, vol. 8, no. 9, p. 15, 2002.

[3] D. I. Babic, K. Streubel, R. P. Mirin, N. M. Margalit, J. E. Bowers, and E. L. Hu, "Transverse-mode and polarization characteristics of double-fused 1.52 μm vertical-cavity lasers," *Electron. Lett.*, vol. 31, pp. 653–654, 1994.

[4] N. M. Margalit, J. Piprek, S. Zhang, D. I. Babic, K. Streubel, R. P. Mirin, J. R. Wesselman, J. E. Bowers, and E. L. Hu, "64°C continuous-wave operation of 1.5-μm vertical-cavity laser," *IEEE J. Select. Topics Quantum Electron.*, vol. 3, pp. 359–365, Apr. 1997.

[5] Y. Ohiso, C. Amano, Y. Itoh, H. Takenouchi, and T. Kurokawa, "Long-wavelength (1.55-μm) vertical-cavity lasers with InGaAsP/InP-Ga/AlAs DBRs by wafer fusion," *IEEE J. Quantum Electron.*, vol. 34, pp. 1904–1913, Oct. 1998.

[6] J. Boucart, C. Starck, F. Gaborit, A. Plais, N. Bouché, E. Derouin, J. C. Remy, J. Bonnet-Gamard, L. Goldstein, C. Fortin, D. Carpentier, P. Salet, F. Brillouet, and J. Jacquet, "Metamorphic DBR and tunnel-junction injection: A CW RT monolithic long-wavelength VCSEL," *IEEE J. Select. Topics Quantum Electron.*, vol. 5, pp. 520–529, May-June 1999.

[7] W. Yuen, G. S. Li, R. F. Nabiev, J. Boucart, P. Kner, J. R. Kner, R. J. Stone, D. Zhang, M. Beaudoin, T. Zheng, C. He, K. Yu, M. Jansen, D. P. Worland, and C. J. Chang-Hasnain, "High-performance 1.6 μm single-epitaxy top-emitting VCSEL," *Electron. Lett.*, vol. 36, no. 13, pp. 1121–1123, June 2000.

[8] S. Rapp, J. Piprek, K. Streubel, J. André, and J. Wallin, "Temperature sensitivity of 1.54-μm vertical-cavity lasers with an InP-based Bragg reflector," *IEEE J. Quantum Electron.*, vol. 33, pp. 1839–1845, Oct. 1997.

[9] M. Ortsiefer, R. Shau, G. Böhm, F. Köhler, and M.-C. Amann, "Low-threshold index-guided 1.5 μm long-wavelength vertical-cavity surface-emitting laser with high efficiency," *Appl. Phys. Lett.*, vol. 76, no. 16, pp. 2179–2181, 2000.

[10] R. Shau, M. Ortsiefer, M. Zigldrum, J. Rosskopf, G. Böhm, F. Köhler, and M.-C. Amann, "Low-threshold InGaAlAs/InP vertical-cavity surface-emitting laser diodes for 1.8-μm wavelength range," *Electron. Lett.*, vol. 36, no. 15, 2000.

[11] E. Hall, S. Nakagawa, G. Almuneau, j. K. Kim, and L. A. Coldren, "Room-temperature, CW operation of lattice-matched long wavelength VCSELs," *Electron. Lett.*, vol. 36, no. 7, 2000.

[12] T. Maier, G. Strasser, and E. Gornik, "Monolithic integration of vertical-cavity laser diodes and resonant photodetectors with hybrid $Si_3N_4 - SiO_2$ top Bragg mirrors," *IEEE Photon. Technol. Lett.*, vol. 12, pp. 119–121, Feb. 2000.

[13] K. Streubel, S. Rapp, J. André, and N. Chitica, "1.26 μm vertical cavity laser with two InP/air-gap reflectors," *Electron. Lett.*, vol. 32, no. 15, 1996.
[14] N. Chitica and M. Strassner, "Room temperature operation of photopumped monolithic InP vertical cavity laser with two air-gap Bragg reflectors," *Appl. Phys. Lett.*, vol. 78, pp. 3935–3937, 2001.
[15] C.-K. Lin, D. Bour, J. Zhu, W. Perez, M. Leary, A. Tandon, S. Corzine, and M. Tan, "High temperature continous-wave operation of 1.3–1.55-μm VCSELs with InP/air-gap DBRs," in *Proc. IEEE LEOS Int. Semiconduct. Laser Conf.*, Garmisch, Germany, 2002, pp. 145–146.
[16] M. C. Larson, B. Pezeshki, and J. S. Harris Jr., "Vertical coupled-cavity microinterferometer on GaAs with deformable-membrane top mirror," *IEEE Photon. Technol. Lett.*, vol. 7, pp. 382–384, Apr. 1995.
[17] E. C. Vail, M. S. Wu, G. S. Li, L. Eng, and C. J. Chang-Hasnain, "GaAs micromachined widely tunable Fabry-Perot filters," *Electron. Lett.*, vol. 31, no. 3, pp. 228–229, 1995.
[18] M. C. Larson, A. R. Massengale, and J. S. Harris, "Continuously tunable micromachined vertical cavity surface emitting laser with 18-nm wavelength range," *Electron. Lett.*, vol. 32, pp. 330–332, 1996.
[19] J. Peerlings, A. Dehé, A. Vogt, M. Tilsch, C. Hebeler, F. Langenhan, P. Meissner, and H. L. Hartnagel, "Long resonator micromachined tunable GaAs-AlAs Fabry–Pérot filter," *IEEE Photon. Technol. Lett.*, vol. 9, pp. 1235–1237, Sept. 1997.
[20] A. Spisser, R. Ledantec, C. Seassal, J. L. Leclercq, T. Benyattou, D. Rondi, R. Blondeau, G. Guillot, and P. Viktorovitch, "Highly selective and widely tunable 1.55-μm InP/Air-Gap micromachined Fabry-Perot filter for optical communications," *IEEE Photon. Technol. Lett.*, vol. 10, pp. 1259–1261, Sept. 1998.
[21] P. Tayebati, P. Wang, M. Azimi, L. Maflah, and D. Vakhshoori, "Microelectromechanical tunable filter with stable half symmetric cavity," *Electron. Lett.*, vol. 34, no. 20, pp. 1967–1968, 1998.
[22] N. Chitica, J. Daleiden, M. Strassner, and K. Streubel, "Monolithic InP-based tunable filter with 10-nm bandwidth for optical data interconnects in the 1550-nm band," *IEEE Photon. Technol. Lett.*, vol. 11, pp. 584–586, May 1999.
[23] N. Chitica, J. Daleiden, J. Bentell, J. André, M. Strassner, S. Greek, D. Pasquariello, M. Karlsson, R. Gupta, and K. Hjort, "Fabrication of tunable InP/Air-gap Fabry-Perot cavities by selective etching of InGaAs sacrificial layers," *Physica Scripta*, vol. T79, pp. 131–134, 1999.
[24] J. Daleiden, N. Chitica, and M. Strassner, "Tunable InP-based microcavity devices for optical communication systems," *Sensors and Materials*, vol. 14, no. 1, pp. 35–45, 2002.
[25] J. Daleiden, V. Rangelov, S. Irmer, F. Römer, M. Strassner, C. Prott, A. Tarraf, and H. Hillmer, "Record tuning range of InP-based multiple air-gap MOEMS filter," *Electron. Lett.*, vol. 38, no. 21, pp. 1270–1271, 2002.
[26] F. Römer, C. Prott, S. Irmer, J. Daleiden, and H. Hillmer, "Tuning efficiency and linewidth of electrostatically actuated multiple air-gap filters," *Appl. Phys. Lett.*, vol. 82, no. 3, 2003.
[27] F. Riemenschneider, M. Aziz, H. Halbritter, I. Sagnes, and P. Meissner, "Low-cost electrothermally tunable optical microcavities based on GaAs," *IEEE Photon. Technol. Lett.*, vol. 14, pp. 1566–1568, Nov. 2002.
[28] M. Y. Li, W. Yuen, G. S. Li, and C. J. Chang-Hasnain, "Top-emitting micromechanical VCSEL with a 31.6-nm tuning range," *IEEE Photon. Technol. Lett.*, vol. 10, pp. 18–20, 1998.
[29] D. Vakhshoori, P. Tayebati, C.-C.Chih-Cheng Lu, M. Azimi, P. Wang, J.-H.Jiang-Huai Zhou, and E. Canoglu, "2-mW CW singlemode operation of a tunable 1550 nm vertical cavity surface emitting laser with 50 nm tuning range," *Electron. Lett.*, vol. 35, pp. 1–2, 1999.
[30] C.-C. Lin, W. A. Martin, and J. S. Harris, "Optomechanical model of surface micromachined tunable optoelectronic devices," *IEEE J. Select. Topics Quantum Electron.*, vol. 8, pp. 80–87, Jan.–Feb. 2002.
[31] A. Tarraf, J. Daleiden, V. Rangelov, F. Römer, C. Prott, S. Irmer, E. Ataro, and H. Hillmer, "A novel low-cost and simple fabrication technology for tunable dielectric air-gap devices," in *SPIE Proc. Series 4945*. Brugge, Belgium: Photonics Fabrication Europe, Oct. 2002.
[32] H. Hillmer, J. Daleiden, S. Irmer, F. Römer, C. Prott, A. Tarraf, M. Strassner, E. Ataro, and T. Scholz, "Potential of micromachined photonics: miniaturization, scaling and applications in continuously tunable vertical air-cavity filters," in *SPIE Proc. Series 4945*. Brugge, Belgium: Photonics Fabrication Europe, Oct. 2002.
[33] S. Irmer, J. Daleiden, V. Rangelov, C. Prott, F. Römer, M. Strassner, A. Tarraf, and H. Hillmer, "Ultralow biased widely continuously tunable Fabry-Pérot filter," *IEEE Photon. Technol. Lett.*, vol. 15, pp. 434–436, Mar. 2002.
[34] L. A. Coldren and S. W. Corzine, *Diode Lasers and Photonic Integrated Circuits*. New York: Wiley, 1995.
[35] N. Chitica, M. Strassner, and J. Daleiden, "Quantitative evaluation of growth-induced residual stress in InP epitaxial micromechanical structures," *Appl. Phys. Lett.*, vol. 77, no. 2, pp. 202–204, 2000.
[36] A. Witzig, M. Streiff, W. Fichtner, F. Römer, C. Prott, and H. Hillmer, "Optical Eigenmodes in VCSEL structures: Spectral portrait and convergence behavior," in *Proc. Conf. Numer. Simulation Semiconduct. Optoelectron. Devices*, Zürich, Switzerland, Sept. 25–27, 2002.
[37] K. H. Huebner, E. A. Thornton, and T. G. Byrom, *The Finite Element Method for Engineers*, 3rd ed. New York: Wiley, 1995.
[38] O. C. Zienkiewicz and R. L. Taylor, *The Finite Element Method*, 4th ed. London: McGraw-Hill, 1994.
[39] S. Adachi, *Physical Properties of III-V Semiconductor Compounds*. New York: Wiley, 1992.
[40] S. D. Senturia, *Microsystem Design*, 4th ed. Norwell, MA: Kluwer, 2002.
[41] E. S. Hung and S. D. Senturia, "Extending the travel range of analog-tuned electrostatic actuators," *J. Microelectromech. Syst.*, vol. 8, no. 4, pp. 497–505, 1999.

Cornelia Prott was born in Marsberg, Germany, in July 1970. She received the Diploma degree in physics from University of Paderborn, Paderborn, Germany, in 1995 and the Ph.D. degree from University of Kassel, Germany, in 1999.

Since 1996, she joined the Technological Electronics in the Institute of Microstructure Technology and Analytics at the University of Kassel, Kassel, Germany, where she is Head of the Modeling and Characterization Group. Her research interests during her thesis work were tunable laser diodes, tuning mechanisms, electroabsorption, and Quantum effects. Her current research concentrates on the design and optimization of microoptical electromechanical systems and tunable vertical cavity devices.

Dr. Prott is a member of the German Physical Society (DPG).

Friedhard Römer was born in Wuppertal, Germany in 1971. He received the Dipl.-Ing. (U) degree with the main focus on optical communications technology from the University of Karlsruhe, Karlsruhe, Germany, in 1996. He is currently pursuing the Ph.D. degree at the University of Kassel, Kassel, Germany.

From 1997 to 1999, he was with the Alcatel SEL Company, Stuttgart, Germany, where he designed telecommunication equipment for cellular radio. In 2000, he joined the Technological Electronics Group, Institute of Microstructure Technologies and Analytics (IMA), University of Kassel. His research areas cover the characterization of vertical cavity lasers as well as the numerical simulations of novel tunable vertical cavity lasers.

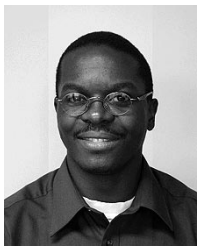

Edwin O. Ataro received the B.Tech. degree (first class honors) in electrical and communication engineering from Moi University, Eldoret, Kenya, in 1989 and the M.Sc. degree in electrical communication engineering from the University of Kassel, Kassel, Germany, in 2000. He is currently putoward a Ph.D. degree at the University of Kassel.

He is presently engaged as a Research Assistant at the Institute of Microstructure Technologies and Analytics (IMA) and Centre for Interdisciplinary Nanostructure Science and Technology (CINSaT), University of Kassel, where his major area of interest is in the simulation and design optimization of vertical cavity photonic devices for dense wavelength-division multiplexing systems.

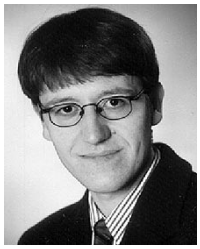

Jürgen Daleiden received the Dipl.-Ing. (1993) and Dr.-Ing. (1997) degree from the Department of Electrical Engineering at the Technical University of Aachen, Germany. In 1994 he joined the Fraunhofer IAF, Freiburg, Germany, where he was working on chemically assisted ion-beam etching of III-V-compound semiconductors for optoelectronic applications (OEICs, high speed, and high power semiconductor lasers). Between 1997 and 1999 he has been with the Royal Institute of Technology (KTH) in Stockholm, Sweden, developing optoelectronic devices in advanced vertical cavity structures and microoptoelectromechanical systems. He was responsible for KTH's part in the ESPRIT-MOEMS project. Since 1999 he is with the Institute of Microstructure Technologies and Analytics (IMA) at the University of Kassel, where he is heading the III/V Technology group. He has authored or co-authored more than 40 publications or conference contributions.

Sören Irmer (S'99) was born in Mühlhausen, Germany, in 1972. He received the M.Sc. degree in applied and modern optics from the University of Reading, Reading, U.K. and Dipl.-Ing. degree (I+II) in electrical engineering from the University of Kassel (Germany) in 1997 and 1998, respectively. In 2000, he joined the technological electronics group at the Institute of Microstructure Technologies and Analytics (IMA) at the University of Kassel where he is currently working toward his Ph.D. degree. His research interests include the design and technology of optical filters.

Amer Tarraf was born in Beyrouth, Lebanon, in 1974. He received the Dipl.-Ing (FH) from the applied university of Konstanz (Germany) and the Dipl.-Ing and M.Sc. in electrical engineering from the University of Kassel (Germany) in 1998 and 2000, respectively. In 2000 he joined the technological electronics group at the Institute of Microstructure Technologies and Analytics (IMA) at the University of Kassel where he is currently working toward his PhD degree. His research interests include the design and technology of organic and inorganic photonic devices.

Hartmut Hillmer, diploma (1985) doctor thesis (1989, summa cum laude) in physics on optically detected electronic transport in Si and III/V QW structures, both in physics from Stuttgart University. From 1989 to 1998 he was with German Telekom Research Center, Darmstadt, and 1991 with NTT Optoelectronics Labs. Atsugi-shi Japan. His habilitation thesis (1996) was on chirped DFB gratings by bent waveguides, ultrafast lasers and MBE growth of AlGaInAs strain-compensated QW laser structures (Darmstadt University). Since 1999 he is full professor in the electrical engineering faculty of Kassel University, Germany, and holds the chair of Technological Electronics. His current research interests are technological implementation, characterization and theoretical model calculations of optoelectronic III/V semiconductor devices: spectral tuning of semiconductor lasers and filters, microsystem technology and nanostructure technology. From 2000 to 2002 he was dean of electrical engineering faculty installing a course in applied computer engineering and is one of the founding members of the Center for Interdisciplinary Nanostructure Science and Technology (CINSaT). He published more than 160 papers, several book chapters, holds ten patents and is a member of the German Physical Society (DPG).